Chemical Geology 567 (2021) 120100

Contents lists available at ScienceDirect

Chemical Geology

journal homepage: www.elsevier.com/locate/chemgeo

Control of V accumulation in organic-rich shales by clay-organic nanocomposites

Zhitong Lu [a,b], Ruizhong Hu [a,b,*], Tao Han [a,b,*], Hanjie Wen [a,b], Bing Mo [a,b], Thomas J. Algeo [c,d,e]

[a] State Key Laboratory of Ore Deposit Geochemistry, Institute of Geochemistry, Chinese Academy of Sciences, Guiyang 550081, China
[b] College of Earth and Planetary Sciences, University of Chinese Academy of Sciences, Beijing 100049, China
[c] Department of Geology, University of Cincinnati, Cincinnati, OH 45221-0013, USA
[d] State Key Laboratory of Geological Processes and Mineral Resources, China University of Geosciences, Wuhan 430074, China
[e] State Key Laboratory of Biogeology and Environmental Geology, China University of Geosciences, Wuhan 430074, China

ARTICLE INFO

Editor: Michael E. Boettcher

Keywords:
Smectite
Illite
Illitization
Vanadium
Niutitang
South China

ABSTRACT

Organic-rich shales exhibit a wide range of vanadium (V) concentrations in deep-time successions. Although V accumulation is generally acknowledged to be related to redox state, organic matter and clay mineral content, previous studies have failed to explain the mechanism of variable V enrichment in organic-rich shales. Here, we hypothesize that clay-organic nanocomposites control authigenic V uptake in organic-rich shales. Specifically, V is scavenged by dissolved organic matter in seawater, which is then taken up by smectite during transport or deposition, followed by V incorporation into illite through illitization of smectite and pyrolysis of organic matter during diagenesis. To test this hypothesis, lower Cambrian black shales from South China were investigated by field emission scanning electron microscopy (FESEM) and transmission electron microscopy (TEM) at a micro- and nanoscale. Results show that only 1M/1M_d-type illite, generated through transformation from a smectite precursor, has significant V concentrations (0.7–4.8 wt%), whereas 2M_1-type illite and other minerals contain little or no V. All 1M/1M_d-type illite was closely associated with organic matter, occurring as clay-organic nanocomposites. Our results are significant in (i) showing clay-organic nanocomposites play a key role in V cycling in the marine system, (ii) providing a mechanism for understanding variations in the V concentrations of deep-time organic-rich shales, and (iii) improving strategies for prospecting and extraction of V ores.

1. Introduction

Vanadium (V), like molybdenum (Mo) and uranium (U), is a highly redox-sensitive element that can be effectively scavenged from seawater under anoxic conditions, and that has been used to study the oxygenation history of the ocean-atmosphere system (Algeo and Maynard, 2004, 2008; Sahoo et al., 2012; Scott et al., 2017). V is commonly present in organic-rich black shales and fossil fuels at concentrations up to thousands of parts per million (ppm) (Lewan and Maynard, 1982; Coveney and Martin, 1983; Kelley et al., 2017; Brough et al., 2019). V-rich black shales have been developed as a non-traditional V source in places such as Nevada, Finland and South China (Zhang et al., 2015; Kelley et al., 2017; Brough et al., 2019). The geochemical cycle of V in the marine system is linked to the redox state of the watermass as well as the availability of host substrates such as organic matter and clay minerals (Breit and Wanty, 1991; Algeo and Maynard, 2004). A conceptual model was proposed in which V(V) was reduced to V(IV) and complexed with organic matter, typically during early diagenesis, after which further reduction to V(III) allowed uptake by illite during late diagenesis (Breit and Wanty, 1991; Peacor et al., 2000; Tribovillard et al., 2006). However, this model did not always conform to the wide range of V concentrations reported for deep-time organic-rich shales (Och et al., 2016). The specific pathways of V incorporation into organic-rich shales remain obscure.

Here, we demonstrate that authigenic V in ancient black shales is hosted mainly by clay-organic nanocomposites, and we hypothesize that this association is the product of a series of events: 1) bonding of aqueous V to dissolved organic matter (DOM) in seawater; 2) formation of clay-organic nanocomposites through adsorption of DOM onto clay-mineral (mainly smectite) surfaces in the water column or at the sediment-water interface; 3) release of V through pyrolysis and conversion of smectite to illite in the deep burial environment; and 4)

* Corresponding author at: State Key Laboratory of Ore Deposit Geochemistry, Institute of Geochemistry, Chinese Academy of Sciences, Guiyang 550081, China.
E-mail addresses: huruizhong@vip.gyig.ac.cn (R. Hu), hantao@mail.gyig.ac.cn (T. Han).

https://doi.org/10.1016/j.chemgeo.2021.120100
Received 14 November 2020; Received in revised form 25 January 2021; Accepted 27 January 2021
Available online 4 February 2021

uptake of V by neoformed illite during the illitization process. This hypothesis is informed by the following observations: 1) the strong affinity of V for organic substances (Lewan and Maynard, 1982; Breit and Wanty, 1991); 2) the intimate association of clays (e.g., smectite, illite) and organic matter (OM) in the form of clay-organic nanocomposites (Kennedy et al., 2002, 2014; Löhr and Kennedy, 2014; Berthonneau et al., 2016); and 3) the common transformation of smectite to illite via the process of illitization in the deep burial environment (Hower et al., 1976; Lynch et al., 1997). To test this hypothesis, we undertook a petrographic and mineralogical study of lower Cambrian black shales in South China using micro-analytical techniques at a micro- and nano-scale. Our results provide new insights into authigenic accumulation, geochemical cycling, and resource exploitation of V in organic-rich shales.

2. Materials and methods

The lower Cambrian Niutitang Formation of South China exhibits a wide range of V concentrations, from hundreds to thousands of parts per million (ppm) (Fig. S1). For this study, a total of 81 fresh samples, including dolomites, cherts, phosphorites and black shales, was collected from the Zhongnan section of Guizhou Province (27°41′22″ N, 106°40′37″ E; n = 37) and Longbizui section of Hunan Province (28°29′53″ N, 109°50′33″ E; n = 44) (Figs. 1 and S1). Secondary oxides, carbonate veinlets and phosphatic nodules were removed prior to grinding, and samples were then powdered to finer than 200 mesh for

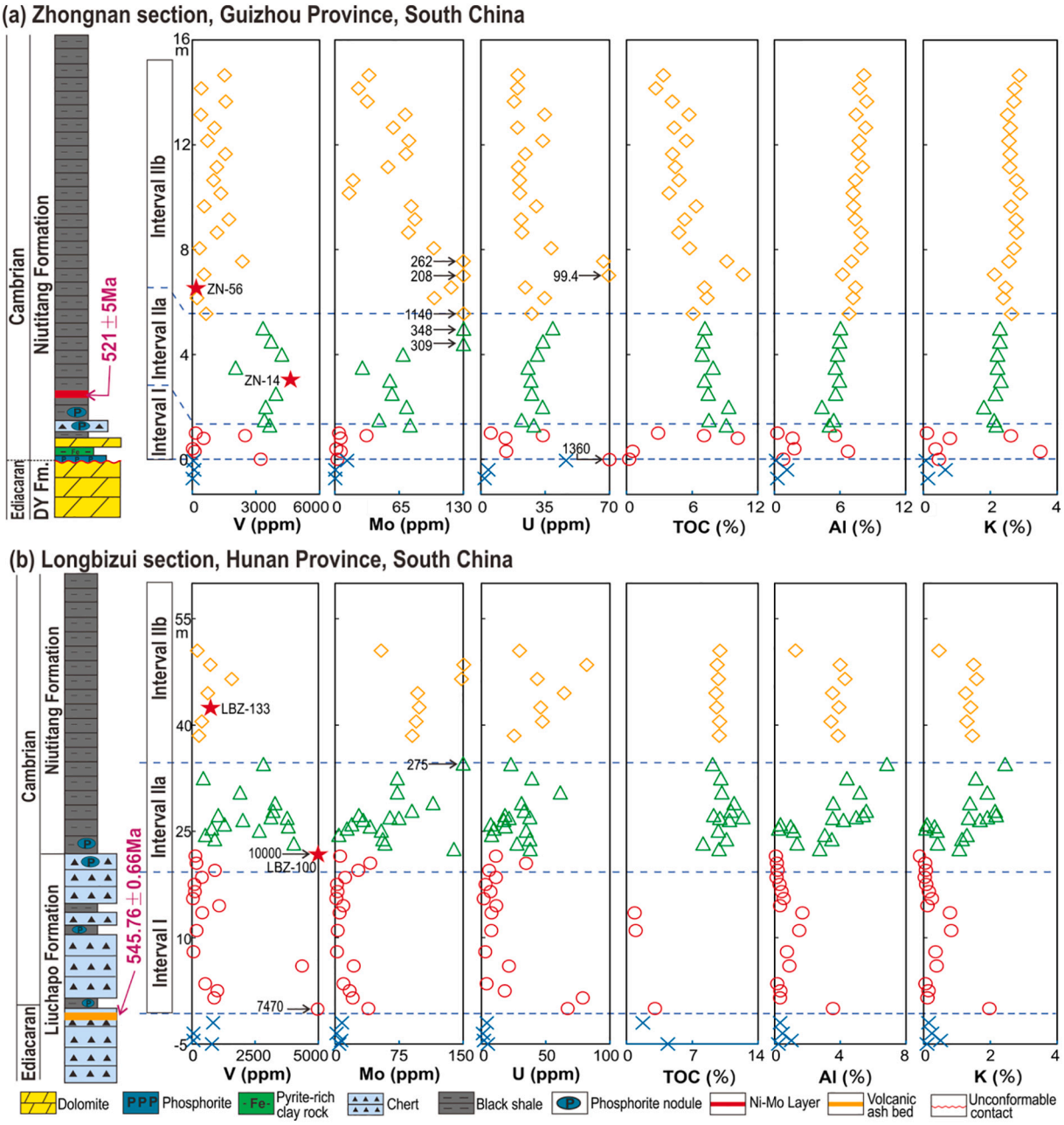

Fig. 1. Distribution of V, Mo, U, Al, K, and TOC in the Zhongnan (a) and Longbizui (b) sections. Interval I, IIa and IIb are marked by red circles, green triangles and orange diamonds, respectively. Samples with abnormally high concentrations are indicated by arrows. The red stars represent samples analyzed by FESEM and TEM (see text). Data for the Longbizui section are from Han et al. (2018). The Re—Os age of the Ni—Mo polymetallic ore layer in the Zhongnan section is from Xu et al. (2011), while the U—Pb age of the volcanic ash bed in the Liuchapo Formation of the Longbizui section is from Yang et al. (2017). Abbreviation: DY Fm. = Dengying Formation. (For interpretation of the references to colour in this figure legend, the reader is referred to the web version of this article.)

major-element analysis by inductively coupled plasma atomic emission spectroscopy (ICP-AES; Agilent 5110) and trace-element analysis by inductively coupled plasma mass spectrometry (ICP-MS; Agilent 7900) at the ALS Chemex Laboratory in Guangzhou, China. Based on multiple analyses (n = 5) of standard reference materials (GBM908-10, MRGeo08, OGGeo08, and OREAS-45e), the accuracy (± 1σ) of our analyses was determined to be better than 3% and 5% for major and trace elements, respectively. The relative standard deviation (i.e., precision) of trace and major element concentrations is <5% (Table S1). Total organic carbon (TOC) contents were analyzed using a vario MACRO Cube element analyzer at the State Key Laboratory of Environmental Geochemistry, Institute of Geochemistry, Chinese Academy of Sciences (IGCAS) with a relative standard deviation better than 5%. Major- and trace-element and TOC data of the Longbizui section (n = 44) are cited from Han et al. (2018).

Selected samples with a range of V concentrations (Fig. 1) were cut

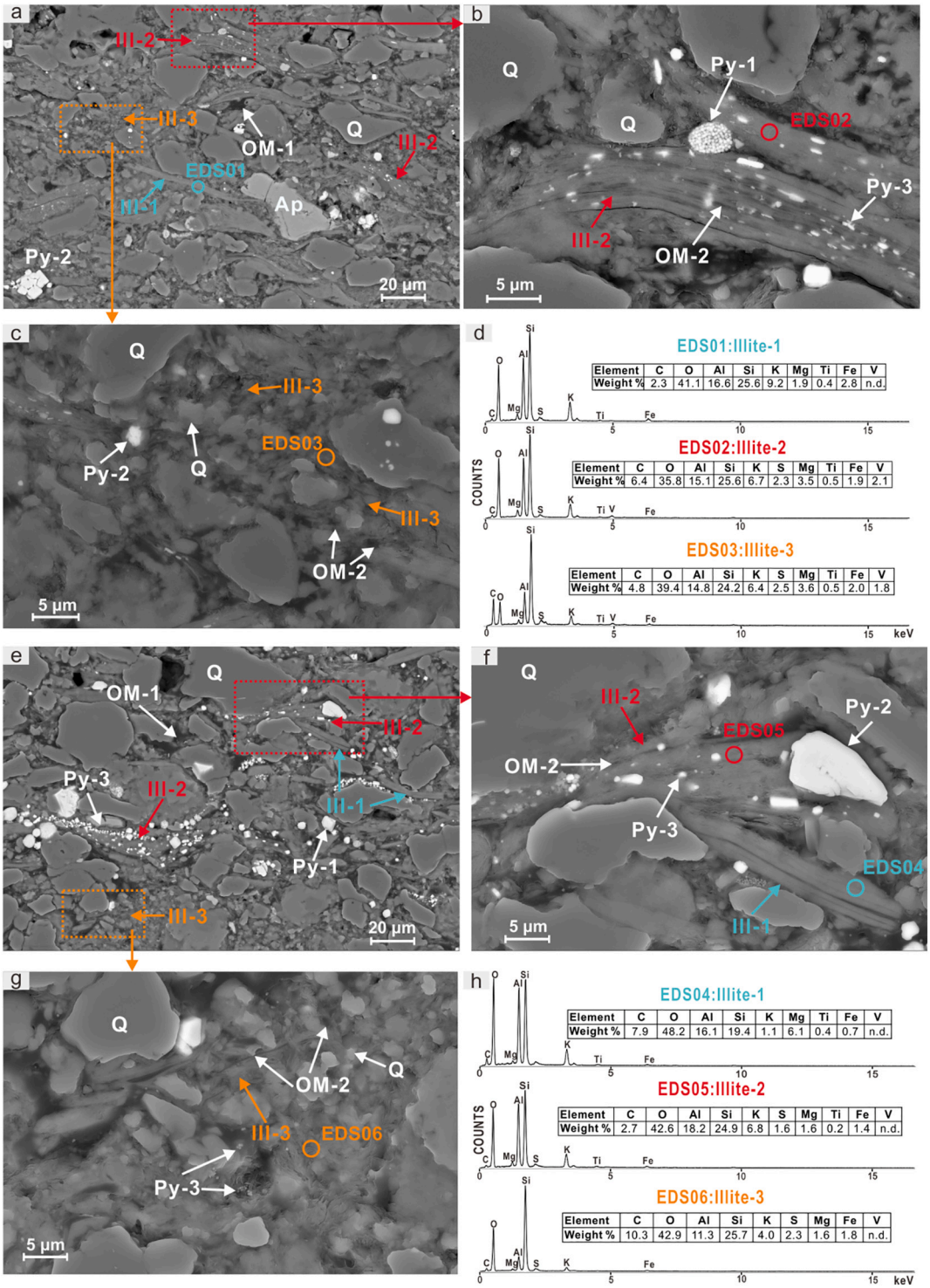

Fig. 2. The petrography and chemical composition of different types of illite, organic matter (OM) and pyrite in a V-rich black shale sample from Interval IIa (a-d; ZN-14, 5190 ppm V) and a V-depleted black shale sample from Interval IIb (e-h; ZN-21, 162 ppm V) of the Zhongnan section. Abbreviations: Q: quartz, Ap: apatite, Ill: illite, Py: pyrite.

and polished for petrographic observations using a FEI Scios DualBeam (i.e., focused ion beam and field emission scanning electron microscopy, FIB-FESEM) equipped with EDAX energy dispersive spectroscopy (EDS) at the Center for Lunar and Planetary Sciences, IGCAS. The FIB-FESEM technique was used to select target areas for transmission electron microscopy (TEM). Detailed petrographic, structural, and chemical analysis of TEM foils (length 10 μm, thickness several tens of nanometers) at a nanoscale was performed using a TECNAI G2 20 TEM equipped with EDAX EDS at the State Key Laboratory for Mineral Deposits Research, Nanjing University. High-resolution TEM images were obtained together with diffraction patterns through selected area electron diffraction (SAED) analysis.

3. Results

3.1. Distribution of V in lower Cambrian black shales

The concentrations of V, Mo, U, Al, K and TOC are given in Table S1

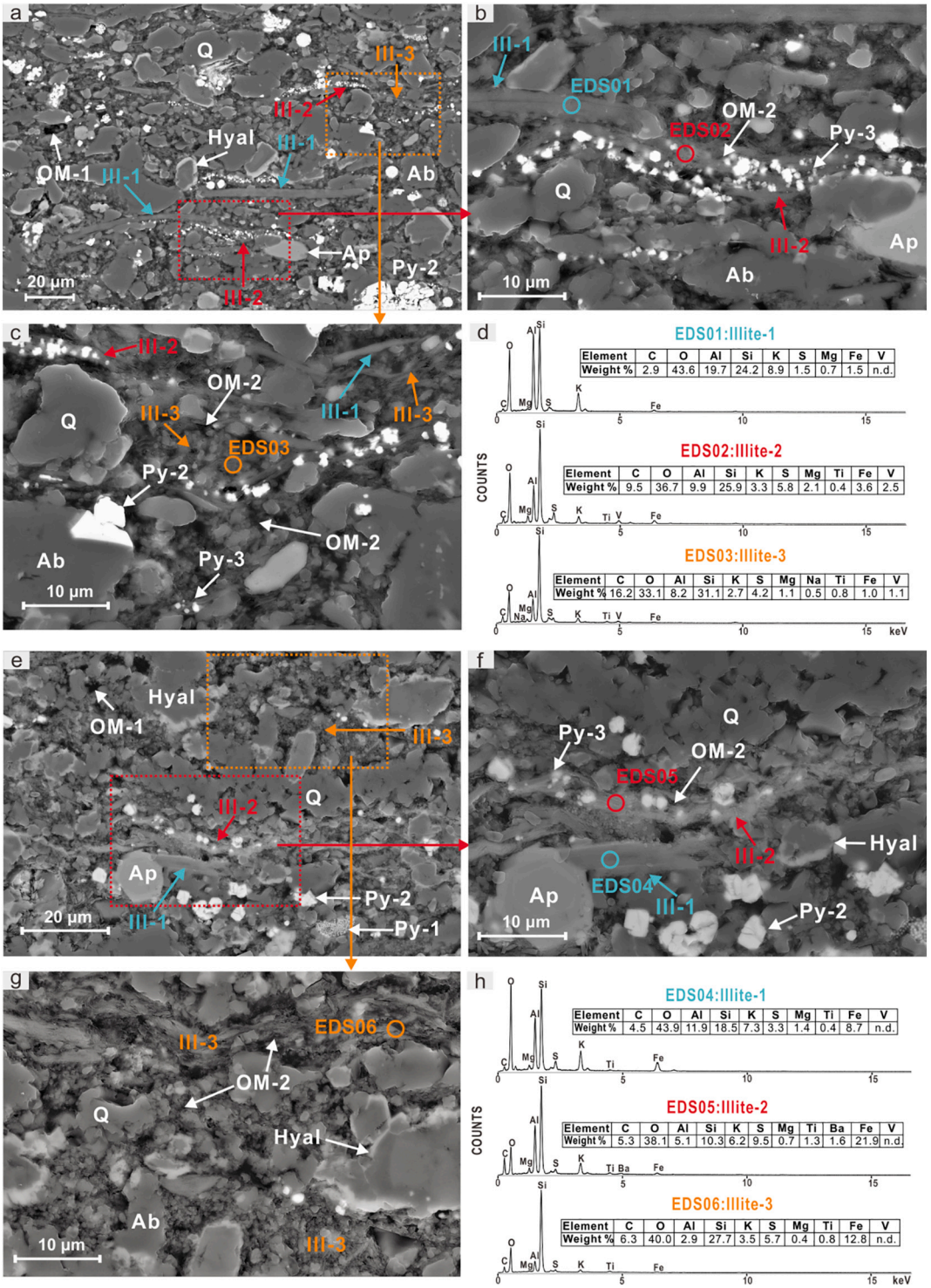

Fig. 3. The petrography and chemical composition of different types of illite, OM and pyrite in a V-rich black shale sample from Interval IIa (a-d; LBZ-100, >10,000 ppm V) and a V-depleted black shale sample from Interval IIb (e-h; LBZ-133, 732 ppm V) of the Longbizui section. Abbreviations: Ab: albite, Hyal: hyalophane.

and shown in Fig. 1. The study sections were previously divided by Han et al. (2018) into two units (Intervals I and II) on the basis of redox conditions as inferred from Mo—U relationships. Specifically, Interval I shows fluctuating Mo—U concentrations owing to accumulation within the Fe—Mn reduction zone (cf. Han et al., 2018; Algeo and Li, 2020). V concentrations are variable at Zhongnan (23–2490 ppm, mean 1150 ppm [note: mean values are geometric means because sample V concentrations exhibit log-normal distributions]) and Longbizui (59–7470 ppm, mean 831 ppm) (Fig. 1 and Table S1). TOC, Al and Fe also exhibit wide concentration ranges due to variable lithology and redox conditions (Fig. 1 and Table S1). Interval II is characterized by higher Mo—U concentrations due to deposition under anoxic conditions (cf. Han et al., 2018). Here, we subdivide this unit into Intervals IIa and IIb on the basis of V concentrations, which are higher in IIa (Zhongnan: 2040–5190 ppm, mean 3630 ppm; Longbizui: 451–10,000 ppm, mean 2100 ppm) than in IIb (Zhongnan: 162–2360 ppm, mean 776 ppm; Longbizui 109–1570 ppm, mean 532 ppm) (Fig. 1 and Table S1). On the other hand, Mo, U, Al, Fe and TOC show similar concentrations in IIa and IIb in both study sections (Fig. 1 and Table S1).

3.2. Petrographic results at micro- and nanoscales

Although a few samples of Interval I have high V concentrations, Interval II exhibits general enrichment of V and other elements (e.g., Mo, U, Al, Fe and TOC) and was therefore chosen as the focus of petrographic observations in this study. For both study sections, the major mineralogic components are quartz, illite, and organic matter, with smaller quantities of pyrite, K-feldspar, albite, and apatite (Figs. 2–4). Hyalophane is present at Longbizui but absent at Zhongnan (Figs. 2 and 3). EDS analysis shows that nearly all V is hosted by illite (0.7–4.8 wt% V), whereas other minerals have no detectable V content (Tables 1 and S2).

Three types of illite were identified in the study sections. The first type (Ill-1) is randomly scattered, large (to tens of microns), lath-shaped detrital illite, which represents the $2M_1$ variety according to its (0,0,1) interplanar spacing of 20.62 Å, as determined by SAED (Figs. 2, 3, 4b, f). The second type (Ill-2) consists of relatively large aggregates (e.g.,

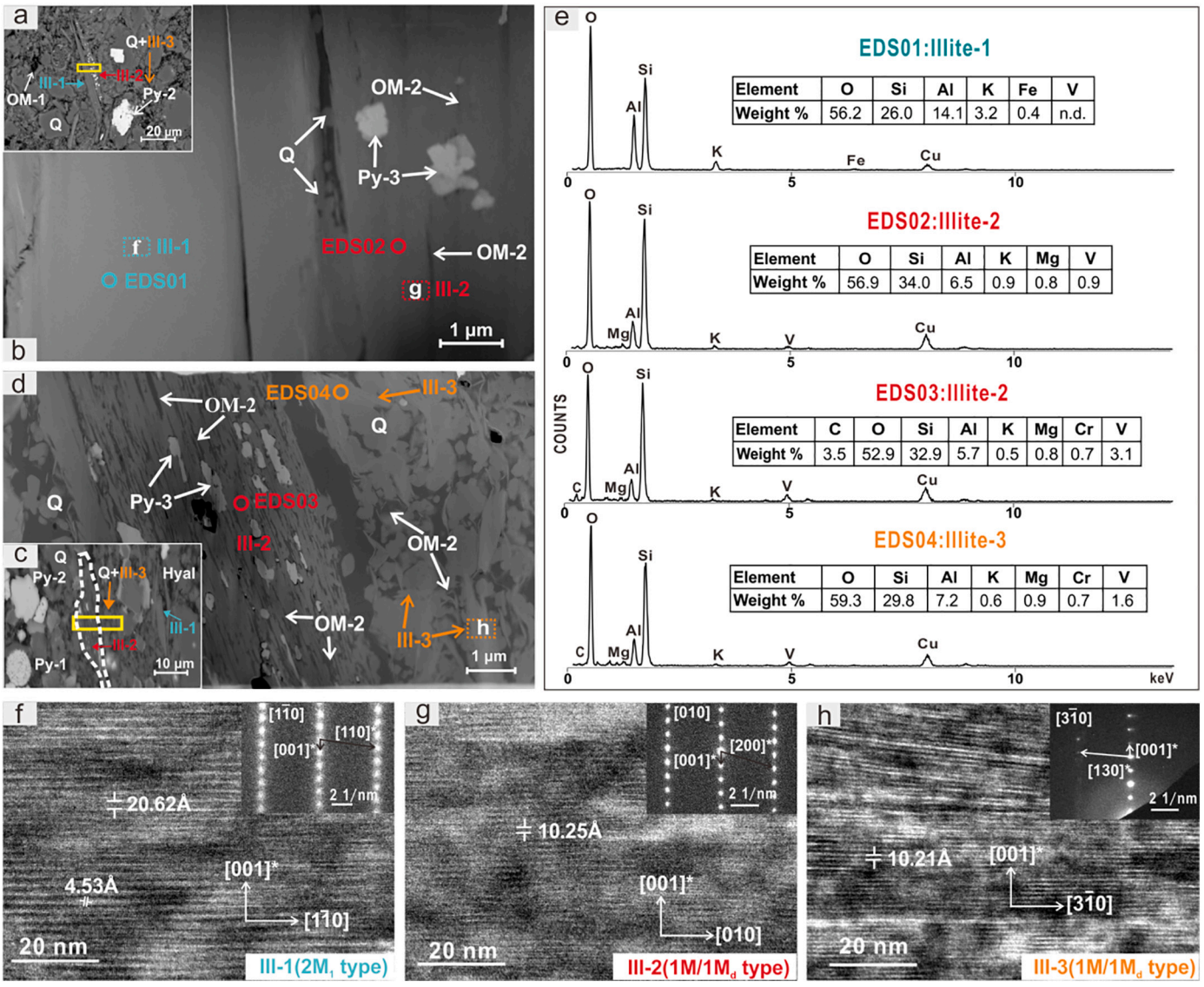

Fig. 4. TEM photos showing nanoscale characteristics of V-rich clay-organic nanocomposites in black shale samples from Interval IIa. (a) and (c) are FESEM-BSE images of different types of illite in Interval IIa of the Zhongnan and Longbizui sections, respectively. (b) and (d) are high angle annular dark field (HAADF) images of TEM foils cut by FIB-FESEM, corresponding to the yellow rectangular areas in (a) and (c), respectively. The green, red and orange dotted rectangles correspond to the HRTEM and SAED regions of Ill-1 (f), Ill-2 (g), and Ill-3 (h), respectively. (e) shows representative TEM-EDS spectra of three types of illite. (For interpretation of the references to colour in this figure legend, the reader is referred to the web version of this article.)

Table 1
V concentrations (wt%) for different types of illite, obtained by FESEM-EDS analysis of Interval IIa and IIb samples from the Zhongnan and Longbizui sections.

Section	Interval	Illite-1	Illite-2	Illite-3
Zhongnan	Interval IIa	n.d.	0.7–4.4 wt% (avg. 1.96 wt%)	0.8–4.8 wt% (avg. 2.08 wt%)
	Interval IIb	n.d.	n.d.	n.d.
Longbizui	Interval IIa	n.d.	1.9–3.7 wt% (avg. 2.70 wt%)	0.8–3.2 wt% (avg. 1.70 wt%)
	Interval IIb	n.d.	n.d.	n.d. ~ 0.2 wt%

Note: n.d. = not detected.

width: 5–10 μm, length: 30–60 μm) of nanoscale illites (25–200 nm) that are closely associated with organic matter and pyrite, and that represents the 1M/1M_d variety with an (0,0,1) interplanar spacing of 10.25 Å (Figs. 2, 3, 4b, g). The third type (Ill-3) is similar to Ill-2 but has a smaller interplanar spacing (10.21 Å) and, more significantly, is somewhat finer in size (e.g., width: 50–500 nm, length: 0.5–2 μm) and more uniformly distributed through the sample matrix (Figs. 2, 3, 4d, h).

EDS analysis demonstrated large variations in V content as a function of stratigraphic interval and type of illite host. No V is present in Ill-1 from either Interval IIa or IIb. In Interval IIa, high V concentrations are associated with both Ill-2 (Zhongnan: 0.7–4.4%; Longbizui: 1.9–3.7%) and Ill-3 (Zhongnan: 0.8–4.8%; Longbizui: 0.8–3.2%) (Figs. 2a-d, 3a-d, Table S2). In Interval IIb, little to no V was detected in either Ill-2 or Ill-3 (Figs. 2e-h, 3e-h, Table S2).

Two types of OM were identified according to mineral assemblage and distribution characteristics. OM-1 consists of organic particles that are tens of microns in diameter and scattered randomly through the sample matrix (Figs. 2a, e, 3a, e, 4b). It has no association with clays and other minerals and probably represents detrital organic material, which is generally refractory and resistant to decay (Menzel and Goering, 1966). OM-2 is much finer in size (10s to 100 s of nm) and is therefore not easily seen in FESEM images (Figs. 2, 3), although it can be seen in HRTEM image (Fig. 4). It is exclusively associated with nanoscale illites in the form of clay-organic nanocomposites (Figs. 4b) commonly parallel to and intercalated with Ill-2 but also discretely distributed around Ill-3 (Fig. 4d). We infer that its origin is from DOM in seawater (see Section 4.2).

Three types of pyrite were also observed. The first type (Py-1) consists of framboidal pyrite crystals with diameters of a few microns, while second type (Py-2) consists of anhedral blocky pyrite crystals of a similar size (Figs. 2-4). Both Py-1 and Py-2 are randomly distributed through the sample matrix. Py-1 is interpreted as fine (~5–10 μm) framboidal pyrite that formed syndepositionally (i.e., in a euxinic water column) or during early diagenesis (Bond and Wignall, 2010). Py-2 formed in the sediment during the early or late diagenesis, often through secondary overgrowths on Py-1 surfaces (Wilkin et al., 1996). The third type (Py-3) consists of nanoscale anhedral pyrite grains that are intimately and exclusively associated with clay-organic nanocomposites (i.e., Ill-2/Ill-3 and OM-2) (Figs. 2–4). These nanoscale pyrite grains are likely to have formed through thermal sulfate reduction of small organic molecules and organosulfur compounds during the pyrolysis of organic matter in conjunction with illitization of smectite in the deep burial environment (Berthonneau et al., 2016).

4. Discussion

4.1. Relationships among clay minerals, organic matter and V

A number of studies have investigated or reviewed clay-organic nanocomposites (Kennedy et al., 2002, 2014; Löhr and Kennedy, 2014; Berthonneau et al., 2016) and V-organic complexes (Breit and Wanty, 1991; Algeo and Maynard, 2004; Tribovillard et al., 2006). Here, we present a brief summary of these topics as a framework for our findings and proposed hypothesis.

Clay minerals are thought to play an important role in organic carbon burial in both modern and ancient depositional systems (Kennedy et al., 2002, 2014; Löhr and Kennedy, 2014; Berthonneau et al., 2016). In modern marine sediments, up to 90% of OM is intimately associated with mineral (e.g., fine clay) surfaces, promoting OM preservation (Mayer, 1994; Keil et al., 1994; Hedges and Keil, 1995; Hemingway et al., 2019). Recalcitrant macro-molecules and particulate organic matter (POM) can also be selectively preserved in sediments (Hatcher et al., 1983; Burdige, 2007). Associations of OM and clay minerals are the product of several processes, including physical sheltering or encapsulation of OM by clay mineral aggregates (Ransom et al., 1998; Salmon et al., 2000), sorption of OM by clay minerals (Keil et al., 1994; Keil and Cowie, 1999; Satterberg et al., 2003; Zimmerman et al., 2004), and intercalation of OM within the interlayer space of expandable clays such as smectite (Kennedy et al., 2002, 2014; Löhr and Kennedy, 2014; Zhu et al., 2020).

Clay-organic nanocomposites form when various types of dissolved OM, including organic micro-molecular and macro-molecular compounds, are adsorbed and/or intercalated with clay minerals, especially with smectite due to its high specific surface area (~700–800 $m^2\ g^{-1}$) (Wang and Lee, 1993; Ding and Henrichs, 2002; Theng, 2012). Evidence for clay-organic nanocomposites includes both strong positive correlations between TOC and mineral surface area (MSA), as well as direct TEM observations at a nanoscale (Kennedy et al., 2002, 2014; Berthonneau et al., 2016). However, clay-organic nanocomposites can be disrupted by illitization of smectite, which is accompanied by collapse of interlayer spaces and expulsion of organic matter (Hower et al., 1976; Lynch et al., 1997; Merriman and Frey, 1999; Lindgreen et al., 2000; Dainyak et al., 2006; Kamp, 2008).

Organic matter shows a strong affinity for V. Strong positive correlations between V and TOC have been noted in many modern and ancient organic-rich shales (Fig. 5a-c; Breit and Wanty, 1991; Algeo and Maynard, 2004; Cruse and Lyons, 2004; Kevin, 2014; Kurzweil et al., 2015). High V concentrations are found in both organic-rich shales (V_2O_5 from 0.18 to 4 wt%) (Kelley et al., 2017; Brough et al., 2019) and heavy oil fractions, in which V occurs mainly as stable vanadyl-porphyrin complexes (Lewan, 1984; Dechaine and Gray, 2010). Although complexation of V(V) with organic compounds (e.g., humic or fulvic acids) is relatively weak (Wehrli, 1987; Huang et al., 2015), reduction to V(IV) or V(III) greatly enhances its uptake by OM. For instance, an experimental study showed that reduction of V(V) to V(IV) was accompanied by a ~50,000-fold increase in complexation by humic acids (Szalay and Szilágyi, 1967). The complexation of V(IV) with OM is linked to reaction of oxygen donor groups (e.g., carboxylate and phenolate) in humic substances (Goodman and Cheshire, 1975; Lu et al., 1998).

4.2. V uptake by clay-organic nanocomposites in Cambrian shales of South China

In lower Cambrian black shales of South China, clay-organic nanocomposites, the primary host of V, are intimately associated with illite and OM at a nanoscale (Figs. 2-4). Not all types of clay minerals and OM can form as clay-organic nanocomposites, which consist almost exclusively of authigenic illite (e.g., Ill-2 and Ill-3) and dissolved OM (e.g., OM-2). Even in clay-organic nanocomposites consisting of these phases, V is not uniformly distributed—it is present in much higher concentrations in association with Ill-2 and Ill-3 of Interval IIa (0.7–4.8%) than of Interval IIb (0–0.2%) (Figs. 1–3; Table 1 and S2). Based on the observations of the present study (Section 3) as well as general relationships among clay minerals, OM, and V (Section 4.1), we will propose a hypothesis regarding its accumulation in lower Cambrian black shales of

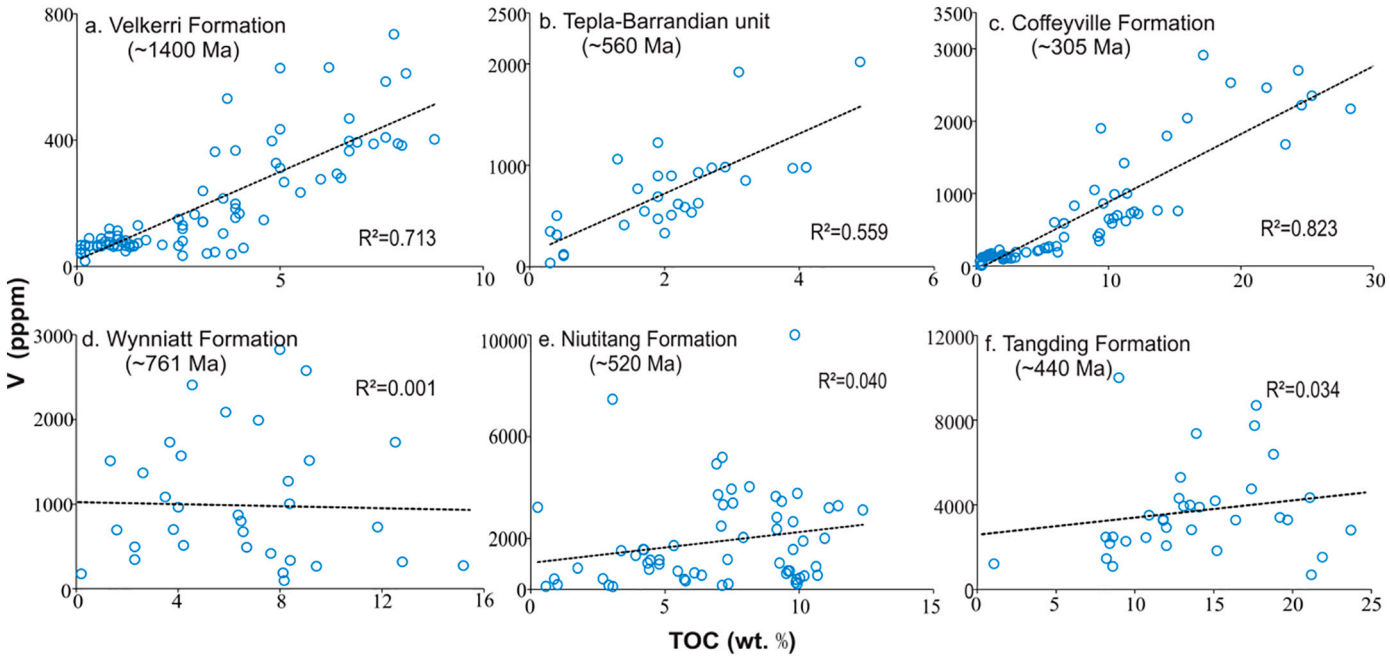

Fig. 5. Scatter plots of V concentration vs. total organic carbon (TOC) for organic-rich shales. (a) Velkerri Formation, Roper Group, Northern Australia (Kevin, 2014); (b) Tepla-Barrandian unit, Czech Republic (Kurzweil et al., 2015); (c) Upper Carboniferous Coffeyville Formation, United States (Cruse and Lyons, 2004); (d) Neoproterozoic Wynniatt Formation, NW Canada (Thomson et al., 2015); (e) Niutitang Formation, South China (this study; Table S1); and (f) Lower Devonian Tangding Formation, South China (Zhang et al., 2015).

South China.

Previous organic geochemical studies concluded that OM in lower Cambrian black shales of South China was sapropelic and sourced mainly from marine cyanobacteria/algae, bacteria, and zooplankton (Kříbek et al., 2007; Gao et al., 2016). We infer that OM-2 is derived from DOM in seawater that was taken up by smectite during deposition and early diagenesis (cf. Wang and Lee, 1993; Ding and Henrichs, 2002; Norde, 2008; Theng, 2012). In modern oceanographic studies, dissolved organic matter (DOM) is defined operationally as particles smaller than <0.2 μm (Eglinton and Murphy, 1969; Hansell and Carlson, 2002) or < 0.45 μm (Chin et al., 1998; Kitis et al., 2001). This size range includes many dissolved organic compounds (e.g., soluble amino acids, fatty acids, carbohydrates, proteins, lipids and humic acids). In the present study units, OM-2 is intercalated with Ill-2 (Fig. 4d, OM monolayer thickness of 5–120 nm) and discretely distributed around illite-3 (Fig. 4d, tens to hundreds of nanometers). The results of adsorption experiments are consistent with the main source of OM in clay-organic nanocomposites being seawater DOM rather than detrital OM, which is generally too large and unreactive (Wang and Lee, 1993; Ding and Henrichs, 2002; Norde, 2008; Theng, 2012).

The formation of clay-organic nanocomposites in black shales is generally accompanied by clay mineral and OM transitions during diagenesis. These relationships between OM and clays (clay-organic nanocomposites) of lower Cambrian black shales are similar to those reported in previous studies except for the dominance of illite (Figs. 2-4) rather than smectite and smectite-illite mixed-layer minerals as in earlier studies (e.g., Kennedy et al., 2014; Löhr and Kennedy, 2014; Bu et al., 2017; Rahman et al., 2017). We infer that the present study units have undergone (near-)complete illitization of smectite during burial diagenesis. This inference is consistent with the high thermal maturity of the study units (equal-Ro > 3.0%; Wang et al., 2016). Additionally, the $1M/1M_d$ type of Ill-2 and Ill-3 with (0,0,1) interplanar spacings of 10.25 Å (Fig. 4g) and 10.21 Å (Fig. 4h) is consistent with those of illitized smectite (Tosca et al., 2010). The occurrence of nanoscale OM-2 arranged either parallel or to Ill-2 and Ill-3 or distributed intergranularly (Fig. 4b, d) was likely a result of OM expulsion linked to collapse of interlayer space in smectite. We infer that OM-2 formed through expulsion of DOM from clay minerals and polymerization to kerogen in deep burial environment. Expulsion of DOM to form nanoscale OM deposits similar to OM-2 has been reported from other formations, e.g., the lower Silurian Longmaxi Formation and the lower Cambrian Lujiaping Formation, Chongqing municipality, South China (Fig. S1; Zhu et al., 2020). Therefore, the presence of illite-organic nanocomposites (i.e., Ill-2/Ill-3 with OM-2) in the lower Cambrian black shales of South China represents an evolution from precursor smectite-organic nanocomposites.

The mineral association and distribution of V in clay-organic nanocomposites can provide insight into V accumulation history. For instance, numerous nanoscale pyrite grains (Py-3) are closely occurred within V-rich clay-organic nanocomposites (e.g., association of Ill-2 and OM-2; Figs. 2b, f, 3b, f, 4d). Because V(IV) can be reduced to V(III) under strongly reducing conditions, such as in the presence of hydrogen sulfide (H_2S) (Wanty et al., 1990; Wanty and Goldhaber, 1992), these nanoscale pyrites may indicate the presence of H_2S during evolution of clay-organic nanocomposites, suggesting the dominated V(III) in clay-organic nanocomposites. Furthermore, in Interval IIa, the Ill-2/Ill-3 in clay-organic nanocomposites contribute higher V concentrations by EDS point analysis and mapping results (Figs. 2b-d, 3b-d, 4a-e and Figs. S2, S3). However, even abundant clay-organic nanocomposites are also presented in Interval IIb, the Ill-2 and Ill-3 has no detectable V (Figs. 2e-h, 3e-h; Tables 1 and S2). Given stable anoxic conditions during Intervals IIa and IIb (Jin et al., 2016; Han et al., 2018), the disappearance of V of Ill-2 and Ill-3 within Interval IIb was caused by a decreased V reservoir, such as a shift from V-enriched to V-depleted seawater in South China during the early Cambrian (Han et al., 2018), related to a basin reservoir effect (Algeo, 2004; Algeo and Lyons, 2006). The effective uptake of V by clay-organic nanocomposites led to a decrease of V reservoir transiently from Interval IIa to IIb in early Cambrian seawater, South China (Fig. 1). This is also consistent with the residence time of V in seawater (e.g., ~50 kyr of V; Algeo, 2004; Tribovillard et al., 2006).

Our results show that clay-organic nanocomposites are the main host for V in lower Cambrian black shales of South China. Based on our

petrographic and geochemical data in combination with existing knowledge regarding clay-organic nanocomposites, we hypothesize a two-stage model of V uptake by these shales (Fig. 6). In the depositional environment, dissolved V(V) was reduced to V(IV) and then complexed by dissolved organic matter in seawater. This V-rich OM was then adsorbed by or intercalated within expandable smectite because of its high specific surface area. Organic host phases provided a bridge between smectite and V, allowing V-rich smectite-organic nanocomposites to form (Fig. 6). During diagenesis, with increasing thermal maturity, illitization of smectite led to conversions to V-rich illite and smectite-illite mixed-layer phases. Concurrent thermal maturation of OM to form kerogen and its subsequent pyrolysis through the oil window led to the release of V from organic phases and its incorporation into the illite lattice. Retention of V may have been facilitated by further reduction of V(IV) to V(III), allowing isomorphous replacement of Al(III) in octahedral sites of the illite structure. Thus, the relative timing of illitization and pyrolysis of OM played a critical role in the redistribution of V in the organic-rich study units during diagenesis.

4.3. Implications for V cycling in marine systems

Our finding that clay-organic nanocomposites represent the main substrate for authigenic V uptake by sediments provide new insight into V cycling in organic-rich shales. First, this inference may resolve as-yet unexplained observations of inconsistent V-OM relationships in organic-rich shales (Kennedy et al., 2002, 2014; Fraser, 2012; Salmon et al., 2000). For instance, a positive correlation exists between V and TOC in some organic-rich shales, but this relationship is not universally manifested (Breit and Wanty, 1991; Algeo and Maynard, 2004; Zhang et al., 2015; Thomson et al., 2015; Fig. 5). The lack of a consistent relationship may reflect the specificity of V-OM associations and the fact that only some formations contain the types of clay-organic nanocomposites prone to strong authigenic V enrichment. Second, although V has been widely used as a paleo-environmental redox proxy, the controls on shifts between its multiple valence states remain poorly understood. Our results are consistent with redox shifts in both the depositional and diagenetic environments, suggesting a more complex relationship between paleo-environmental conditions and authigenic V enrichment than is generally acknowledged. Third, the V removal efficiency of clay-organic nanocomposites may have transiently depleted seawater V, as during deposition of Interval IIb in the present study, when the concentration of aqueous V, but not that of Mo or U, was sharply drawn down (Fig. 1). Finally, the V isotopic composition of bulk samples should prove to be a useful paleo-environmental proxy because it records primary marine conditions that are not influenced by the basin reservoir effect or subsequently modified by diagenesis.

4.4. Implications for V prospecting and extraction from black shale deposits

V is a critical metal for the transition to a low-carbon economy, having a wide range of prospective applications (Huang et al., 2015; Rehder, 2016). After vanadiferous titanomagnetite deposits, organic-rich black shales are the second most important ore of V (Zhang et al., 2015; Kelley et al., 2017; Brough et al., 2019). Our findings of clay-organic nanocomposites controlling V accumulation in organic-rich shales have implications for prospecting of V-rich black shale deposits and subsequent V extraction. First, our results show that not all black shales are enriched in V because both the formation of clay-organic nanocomposites and the availability of seawater V under anoxic conditions are key factors in V enrichment. Furthermore, high rates of V removal to the sediment, which can strongly deplete the seawater V reservoir, tend to result in relatively higher and lower V concentrations in the lower and upper parts of a black shale succession, respectively, as seen in Intervals IIa and IIb in the present study (Fig. 1). Black shale sections in different sedimentary facies of South China also show this same vertical pattern of V distribution (Fig. S1). Therefore, the lower parts of black shale successions represent a relatively more promising target for V prospecting. Second, our results also provide insights into optimization of V extraction procedures. The current procedure for extraction of V from organic-rich shale assumes that illite is the host mineral for V, and therefore roasting, floatation and acid-leaching steps are applied (Wang et al., 2014; Liu et al., 2017). Our results reveal that more coarsely crystalline detrital illite contains little to no V but that nanoscale illite transformed from smectite contains substantial V (Figs. 2–4). Thus, the gravity separation and classification-flotation

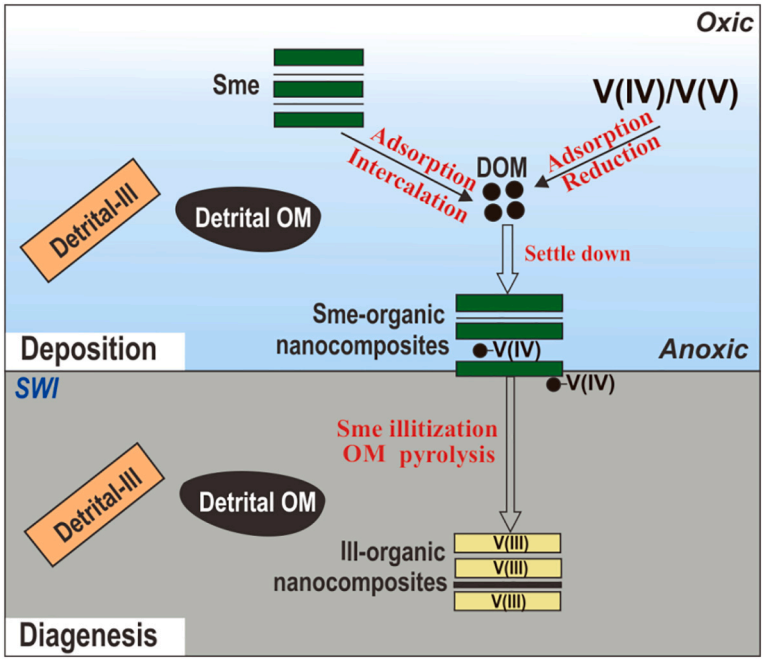

Fig. 6. A comprehensive model for the formation and preservation of V-rich clay-organic nanocomposites during deposition and diagenesis of organic-rich shales. Abbreviations: DOM: dissolved organic matter, Sme: smectite, Ill: illite, SWI: sediment-water interface.

steps used to separate V-bearing illite from other minerals can be optimized based on illite crystal size data. Also, the intimate association of nanoscale illite, OM and pyrite in clay-organic composites affects the flotation efficiency of V-bearing illite and requires greater acid consumption during leaching. Therefore, a roasting step should be added at the beginning of the extraction procedure. Lastly, due to the presence of nanoscale pyrite in V-rich clay-organic nanocomposites, liberation of Fe ions into the acid-leaching solution will affect the purity of the final V-product. For this reason, a weak acid (e.g., oxalic acid) is superior to sulfuric acid, as now widely used in the acid-leaching step.

5. Conclusions

A conceptual model for control of V accumulation in organic-rich shales by clay-organic nanocomposites is herein proposed and tested for lower Cambrian formations in South China based on elemental geochemical and microscopic petrographic analyses. This model can account for variable incorporation of V into organic-rich shales and thus explains secular variation in the V content of ancient black shales.

Especially, three types of illite with $2M_1$ type of Ill-1 and $1M/1M_d$ type of Ill-2 and Ill-3 were identified in this study. The clay-organic nanocomposites (e.g., intimate association of Ill-2/Ill-3 and organic matter) are the predominant carriers for the V accumulation in organic-rich shales. Dissolved organic matter plays a bridge function for the reduction and complexion of V(IV) and its adsorption/intercalation by smectite during deposition, yielding V-rich smectite-organic nanocomposites. Subsequently, smectite illitization and pyrolysis of organic matter promote V release and incorporation into illite as V(III) during diagenesis, yielding V-rich illite-organic nanocomposites. Our results not only demonstrate the importance of formation of clay-organic nanocomposites as a control on V accumulation in organic-rich shales, but also provide basic information for the robust use of V as a redox proxy, and for prospecting and extraction of V from organic-rich shales.

Declaration of Competing Interest

None.

Acknowledgments

Many thanks give to Dr. Jiani Chen and Shirong Liu for support with the TEM analysis, to Dr. Zhuang Guo for TEM data processing, and to Richard B. Wanty and another anonymous reviewer for their insightful reviews. This study was funded by the National Natural Science Foundation of China (U1812402, 41830432, 41673053, 41890841) and the Strategic Priority Research Program (B) of Chinese Academy of Sciences (XDB18030300).

Appendix A. Supplementary data

Supplementary data to this article can be found online at https://doi.org/10.1016/j.chemgeo.2021.120100.

References

Algeo, T.J., 2004. Can marine anoxic events draw down the trace element inventory of seawater? Geology 32, 1057–1060. https://doi.org/10.1130/G20896.

Algeo, T.J., Li, C., 2020. Redox classification and calibration of redox thresholds in sedimentary systems. Geochim. Cosmochim. Acta 287, 8–26. https://doi.org/10.1016/j.gca.2020.01.055.

Algeo, T.J., Lyons, T.W., 2006. Mo–total organic carbon covariation in modern anoxic marine environments: implications for analysis of paleoredox and paleohydrographic conditions. Paleoceanography 21, 1–23. https://doi.org/10.1029/2004PA001112.

Algeo, T.J., Maynard, J.B., 2004. Trace element behavior and redox facies in core shales of Upper Pennsylvanian Kansas-type cyclothems. Chem. Geol. 206, 289–318. https://doi.org/10.1016/j.chemgeo.2003.12.009.

Algeo, T.J., Maynard, J.B., 2008. Trace-metal covariation as a guide to water-mass conditions in ancient anoxic marine environments. Geosphere 4, 872–887. https://doi.org/10.1130/ges00174.1.

Berthonneau, J., Grauby, O., Abuhaikal, M., Pellenq, R.J., Ulm, F.J., Van Damme, H., 2016. Evolution of organo-clay composites with respect to thermal maturity in type II organic-rich source rocks. Geochim. Cosmochim. Acta 195, 68–83. https://doi.org/10.1016/j.gca.2016.09.008.

Bond, D.P.G., Wignall, P.B., 2010. Pyrite framboid study of marine Permian: Triassic boundary sections: a complex anoxic event and its relationship to contemporaneous mass extinction. Geol. Soc. Am. Bull. 122, 1265–1279. https://doi.org/10.1130/B30042.1.

Breit, G.N., Wanty, R.B., 1991. Vanadium accumulation in carbonaceous rocks-a review of geochemical controls during deposition and diagenesis. Chem. Geol. 91, 83–97. https://doi.org/10.1016/0009-2541(91)90083-4.

Brough, C., Bowell, R.J., Larkin, J., 2019. The geology of vanadium deposits. In: Bowell, R. (Ed.), An Introduction to Vanadium. Nova Science Publishers, Inc, pp. 87–117.

Bu, H., Yuan, P., Liu, H., Liu, D., Liu, J., He, H., Zhou, J., Song, H., Li, Z., 2017. Effects of complexation between organic matter OM. and clay mineral on OM pyrolysis. Geochim. Cosmochim. Acta 212, 1–15. https://doi.org/10.1016/j.gca.2017.04.045.

Burdige, D.J., 2007. Preservation of organic matter in marine sediments: controls, mechanisms, and an imbalance in sediment organic carbon budgets? Chem. Rev. 107, 467–485. https://doi.org/10.1021/cr050347q.

Chin, W.C., Orellana, M.V., Verdugo, P., 1998. Spontaneous assembly of marine dissolved organic matter into polymer gels. Nature 391, 568–572. https://doi.org/10.1038/35345.

Coveney, R.M., Martin, S.P., 1983. Molybdenum and other heavy metals of the Mecca Quarry and Logan Quarry shales. Econ. Geol. 78, 132–149. https://doi.org/10.2113/gsecongeo.78.1.132.

Cruse, A.M., Lyons, T.W., 2004. Trace metal records of regional paleoenvironmental variability in Pennsylvanian (Upper Carboniferous) black shales. Chem. Geol. 206, 319–345. https://doi.org/10.1016/j.chemgeo.2003.12.010.

Dainyak, L.G., Drits, V.A., Zviagina, B.B., Lindgreen, H., 2006. Cation redistribution in the octahedral sheet during diagenesis of illite-smectites from Jurassic and Cambrian oil source rock shales. Am. Mineral. 91, 589–603. https://doi.org/10.2138/am.2006.2047.

Dechaine, G.P., Gray, M.R., 2010. Chemistry and association of vanadium compounds in heavy oil and bitumen, and implications for their selective removal. Energy Fuel 24, 2795–2808. https://doi.org/10.1021/ef100173j.

Ding, X., Henrichs, S.M., 2002. Adsorption and desorption of proteins and polyamino acids by clay minerals and marine sediments. Mar. Chem. 77, 225–237. https://doi.org/10.1016/S0304-4203(01)00085-8.

Eglinton, G., Murphy, M.T.J., 1969. Organic Geochemistry: Methods and Results (828 pp.).

Fraser, S.A., 2012. Nanoscale Imaging of the Woodford Shale, Oklahoma, USA: Organic Matter Preservation as Clay-organic Nanocomposites. Ph.D. thesis. University of Adelaide, Australia (61 pp.).

Gao, P., Liu, G., Jia, C., Young, A., Wang, Z., Wang, T., Zhan, P., Wang, D., 2016. Redox variations and organic matter accumulation on the Yangtze carbonate platform during Late Ediacaran-Early Cambrian: constraints from petrology and geochemistry. Palaeogeogr. Palaeoclimatol. Palaeoecol. 450, 91–110. https://doi.org/10.1016/j.palaeo.2016.02.058.

Goodman, B.A., Cheshire, M.V., 1975. The bonding of vanadium in complexes with humic acid: an electron paramagnetic resonance study. Geochim. Cosmochim. Acta 39, 1711–1713. https://doi.org/10.1016/0016-7037(75)90093-9.

Han, T., Fan, H., Wen, H., 2018. Dwindling vanadium in seawater during the early Cambrian, South China. Chem. Geol. 492, 20–29. https://doi.org/10.1016/j.chemgeo.2018.05.022.

Hansell, D.A., Carlson, C.A., 2002. Biogeochemistry of Marine Dissolved Organic Matter. Academic Press (667 pp.).

Hatcher, P.G., Spiker, E.C., Szeverenyi, N.M., Maciel, G.E., 1983. Selective preservation and origin of petroleum-forming aquatic kerogen. Nature 305, 498–501. https://doi.org/10.1038/305498a0.

Hedges, J.H., Keil, H.G., 1995. Sedimentary organic matter preservation: an assessment and speculative synthesis. Mar. Chem. 49, 81–115. https://doi.org/10.1016/0304-4203(95)00008-F.

Hemingway, J.D., Rothman, D.H., Grant, K.E., Rosengard, S.Z., Eglinton, T.I., Derry, L.A., Derry, L.A., Galy, V.V., 2019. Mineral protection regulates long-term global preservation of natural organic carbon. Nature 570, 228–231. https://doi.org/10.1038/s41586-019-1280-6.

Hower, J., Eslinger, E., Hower, M.E., Perry, E.A., 1976. Mechanism of burial metamorphism of argillaceous sediment. Mineralogical and chemical evidence. Geol. Soc. Am. Bull. 87, 725–737. https://doi.org/10.1130/0016-7606(1976)872.0.CO;2.

Huang, J.H., Huang, F., Evans, L., Glasauer, S., 2015. Vanadium: global (bio) geochemistry. Chem. Geol. 417, 68–89. https://doi.org/10.1016/j.chemgeo.2015.09.019.

Jin, C., Li, C., Algeo, T.J., Planavsky, N.J., Cui, H., Yang, X., Zhao, Y., Zhang, X., Xie, S., 2016. A highly redox-heterogeneous ocean in South China during the early Cambrian ~529–514 Ma.: implications for biota-environment co-evolution. Earth Planet. Sci. Lett. 441, 38–51. https://doi.org/10.1016/j.epsl.2016.02.019.

Kamp, P.C.V.D., 2008. Smectite-illite-muscovite transformations, quartz dissolution, and silica release in shales. Clay Clay Miner. 56, 66–81. https://doi.org/10.1346/CCMN.2008.0560106.

Keil, R.G., Cowie, G.L., 1999. Organic matter preservation through the oxygen-deficient zone of the NE Arabian Sea as discerned by organic carbon: mineral surface area ratios. Mar. Geol. 161, 13–22. https://doi.org/10.1016/S0025-3227(99)00052-3.

Keil, R.G., Montlucon, D.B., Prahl, F.G., Hedges, J., 1994. Sorptive preservation of labile organic matter in marine sediments. Nature 370, 549–552. https://doi.org/10.1038/370549a0.

Kelley, K.D., Scott, C.T., Polyak, D.E., Kimball, B.E., 2017. Vanadium. In: Schulz, K.J., DeYoung Jr., J.H., Seal II, R.R., Bradley, D.C. (Eds.), Critical Mineral Resources of the United States-Economic and Environmental Geology and Prospects for Future Supply. U.S. Geological Survey Professional Paper, 1802, pp. U1–U36.

Kennedy, M.J., Pevear, D.R., Hil, R.J., 2002. Mineral surface control of organic carbon in black shale. Science 295, 657–660. https://doi.org/10.1126/science.1066611.

Kennedy, M.J., Löhr, S.C., Fraser, S.A., Baruch, E.T., 2014. Direct evidence for organic carbon preservation as clay-organic nanocomposites in a Devonian black shale; from deposition to diagenesis. Earth Planet. Sci. Lett. 388, 59–70. https://doi.org/10.1016/j.epsl.2013.11.044.

Kevin, D.N., 2014. A Geochemical Study of the 1.4 Ga Roper Group, Northern Australia: A Window to Environmental Conditions and Life During the Mid-Proterozoic. Ph.D. dissertation. University of California, Riverside, Riverside, California (45 pp.).

Kitis, M., Kilduff, J.E., Karanfil, T., 2001. Isolation of dissolved organic matter (DOM) from surface waters using reverse osmosis and its impact on the reactivity of DOM to formation and speciation of disinfection by-products. Water Res. 35, 2225–2234. https://doi.org/10.1016/S0043-1354(00)00509-1.

Kříbek, B., Sykorová, I., Pašava, J., Machovič, V., 2007. Organic geochemistry and petrology of barren and Mo-Ni-PGE mineralized marine black shales of the lower Cambrian Niutitang Formation South China. Int. J. Coal Geol. 72, 240–256. https://doi.org/10.1016/j.coal.2007.02.002.

Kurzweil, F., Drost, K., Pasava, J., Wille, M., Taubald, H., Schoeckle, D., Schoenberg, R., 2015. Coupled sulfur, iron and molybdenum isotope data from black shales of the Teplá-Barrandian unit argue against deep ocean oxygenation during the Ediacaran. Geochim. Cosmochim. Acta 171, 121–142. https://doi.org/10.1016/j.gca.2015.08.022.

Lewan, M.D., 1984. Factors controlling the proportionality of vanadium to nickel in crude oils. Geochim. Cosmochim. Acta 48, 2231–2238. https://doi.org/10.1016/0016-7037(84)90219-9.

Lewan, M.D., Maynard, J.B., 1982. Factors controlling enrichment of vanadium and nickel in the bitumen of organic sedimentary rocks. Geochim. Cosmochim. Acta 46, 2547–2560. https://doi.org/10.1016/0016-7037(82)90377-5.

Lindgreen, H., Drits, V.A., Sakharov, B.A., Salyn, A.L., Wrang, P., Dainyak, L.G., 2000. Illite-smectite structural changes during metamorphism in black Cambrian Alum shales from the Baltic area. Am. Mineral. 85, 1223–1238. https://doi.org/10.2138/am-2000-8-916.

Liu, C., Zhang, Y.M., Bao, S.X., 2017. Vanadium recovery from stone coal through roasting and flotation. Trans. Nonferrous Metals Soc. China 027, 197–203. https://doi.org/10.1016/S1003-6326(17)60022-0.

Löhr, S.C., Kennedy, M.J., 2014. Organomineral nanocomposite carbon burial during Oceanic Anoxic Event 2. Biogeoences 11, 4971–4983. https://doi.org/10.5194/bg-11-4971-2014.

Lu, X.Q., Johnson, W.D., Hook, J., 1998. Reaction of vanadate with aquatic humic substances: an ESR and V-51 NMR study. Environ. Sci. Technol. 32, 2257–2263. https://doi.org/10.1021/es970930r.

Lynch, F.L., Mack, L.E., Land, L.S., 1997. Burial diagenesis of illite/smectite in shales and the origins of authigenic quartz and secondary porosity in sandstones. Geochim. Cosmochim. Acta 61, 1995–2006. https://doi.org/10.1016/S0016-7037(97)00066-5.

Mayer, L.M., 1994. Surface area control of organic carbon accumulation in continental shelf sediments. Geochim. Cosmochim. Acta 58, 1271–1284. https://doi.org/10.1016/0016-7037(94)90381-6.

Menzel, D.W., Goering, J.J., 1966. The distribution of organic detritus in the ocean. Limnol. Oceanogr. 113, 333–337. https://doi.org/10.4319/lo.1966.11.3.0333.

Merriman, R.J., Frey, M., 1999. Patterns of very low-grade metamorphism in metapelitic rocks. In: Frey, M., Robinson, D. (Eds.), Low Grade Metamorphism. Blackwell Science Ltd., Oxford, UK (313 pp.).

Norde, W., 2008. Adsorption of biopolymers, with special emphasis on globular proteins. In: Huang, Q., Huang, P.M., Violante, A. (Eds.), Soil Mineral-microbe-organic Interactions. Springer-Verlag, Berlin, pp. 99–123.

Och, L.M., Cremonese, L., Shields-Zhou, G.A., Poulton, S.W., Struck, U., Ling, H., Li, D., Chen, X., Manning, C., Thirlwall, M., Strauss, H., Zhu, M., 2016. Palaeoceanographic controls on spatial redox distribution over the Yangtze Platform during the Ediacaran-Cambrian transition. Sedimentology 63, 378–410. https://doi.org/10.1111/sed.12220.

Peacor, D.R., Coveney, R.M., Zhao, G., 2000. Authigenic illite and organic matter: the principal hosts of vanadium in the Mecca Quarry shale at Velpen, Indiana. Clay Clay Miner. 48, 311–316. https://doi.org/10.1346/CCMN.2000.0480301.

Rahman, H.M., Kennedy, M.J., Löhr, S.C., Dewhurst, D.N., 2017. Clay-organic association as a control on hydrocarbon generation in shale. Org. Geochem. 105, 42–55. https://doi.org/10.1016/j.orggeochem.2017.01.011.

Ransom, B., Kim, D., Kastner, M., Wainwright, S., 1998. Organic matter preservation on continental slopes: importance of mineralogy and surface area. Geochim. Cosmochim. Acta 62, 1329–1345. https://doi.org/10.1016/S0016-7037(98)00050-7.

Rehder, D., 2016. Vanadium. Reference Module in Chemistry. Molecular Sciences and Chemical Engineering, pp. 1–11. https://doi.org/10.1016/B978-0-12-409547-2.11411-8.

Sahoo, S.K., Planavsky, N.J., Kendall, B., Wang, X., Shi, X., Scott, C., Anbar, A.D., Lyons, T.W., Jiang, G., 2012. Ocean oxygenation in the wake of the Marinoan glaciation. Nature 489, 546–549. https://doi.org/10.1525/awr.1984.5.4.54.

Salmon, V., Derenne, S., Lallier-Verges, E., Largeau, C., Beaudoin, B., 2000. Protection of organic matter by mineral matrix in a Cenomanian black shale. Org. Geochem. 31, 463–474. https://doi.org/10.1016/S0146-6380(00)00013-9.

Satterberg, J., Arnarson, T.S., Lessard, E.J., Keil, R.G., 2003. Sorption of organic matter from four phytoplankton species to montmorillonite, chlorite and kaolinite in seawater. Mar. Chem. 81, 11–18. https://doi.org/10.1016/S0304-4203(02)00136-6.

Scott, C., Slack, J.F., Kelley, K.D., 2017. The hyperenrichment of V and Zn in black shales of the Late Devonian-Early Mississippian Bakken Formation (USA). Chem. Geol. 452, 24–33. https://doi.org/10.1016/j.chemgeo.2017.01.026.

Szalay, A., Szilágyi, M., 1967. The association of vanadium with humic acids. Geochim. Cosmochim. Acta 31, 1–6. https://doi.org/10.1016/0016-7037(67)90093-2.

Theng, B.K.G., 2012. Formation and Properties of Clay-polymer Complexes. Developments in Clay Science. Amsterdam, Elsevier (511 pp.).

Thomson, D., Rainbird, R.H., Planavsky, N., Lyons, T.W., Bekker, A., 2015. Chemostratigraphy of the Shaler Supergroup, Victoria Island, NW Canada: a record of ocean composition prior to the Cryogenian glaciations. Precambrian Res. 263, 232–245. https://doi.org/10.1016/j.precamres.2015.02.007.

Tosca, N.J., Johnston, D.T., Mushegian, A., Rothman, D.H., Summons, R.E., Knoll, A.H., 2010. Clay mineralogy, organic carbon burial, and redox evolution in Proterozoic oceans. Geochim. Cosmochim. Acta 74, 1579–1592. https://doi.org/10.1016/j.gca.2009.12.001.

Tribovillard, N., Algeo, T.J., Lyons, T., Riboulleau, A., 2006. Trace metals as paleoredox and paleoproductivity proxies: an update. Chem. Geol. 232, 12–32. https://doi.org/10.1016/j.chemgeo.2006.02.012.

Wang, X., Lee, C., 1993. Adsorption and desorption of aliphatic amines, amino acids and acetate by clay minerals and marine sediments. Mar. Chem. 44, 1–23. https://doi.org/10.1016/0304-4203(93)90002-6.

Wang, F., Zhang, Y.M., Liu, T., Huang, J., Liu, J., 2014. Comparison of direct acid leaching process and blank roasting acid leaching process in extracting vanadium from stone coal. Int. J. Miner. Process. 128, 40–47. https://doi.org/10.1016/j.minpro.2013.12.010.

Wang, Y., Gu, Y., Ding, W., Gong, D., Yin, S., Wang, X., Zhou, X., Zhou, X., Xiao, Z., Gui, Z., 2016. Characteristics and dominant controlling factors of organic-rich marine shales with high thermal maturity: a case study of the lower Cambrian Niutitang Formation in the Cen'gong block, Southern China. J. Nat. Gas Sci. Eng. 33, 81–96. https://doi.org/10.1016/j.jngse.2016.05.009.

Wanty, R.B., Goldhaber, M.B., 1992. Thermodynamics and kinetics of reactions involving vanadium in natural systems: accumulation of vanadium in sedimentary rocks. Geochim. Cosmochim. Acta 56, 1471–1483. https://doi.org/10.1016/0016-7037(92)90217-7.

Wanty, R.B., Goldhaber, M.B., Northrop, H.R., 1990. Geochemistry of vanadium in an epigenetic sandstone-hosted vanadium-uranium deposit, Henry basin, Utah. Econ. Geol. 85, 270–284. https://doi.org/10.2113/gsecongeo.85.2.270.

Wehrli, B., 1987. Vanadium in der Hydrosphäre; Oberflächenkomplexe und Oxidationskinetik. Ph.D. dissertation. Eidgenossische Technische Hochschule ETH, Zurich, Switzerland (129 pp.).

Wilkin, R.T., Barnes, H.L., Brantley, S.L., 1996. The size distribution of framboidal pyrite in modern sediments: an indicator of redox conditions. Geochim. Cosmochim. Acta 60, 3897–3912. https://doi.org/10.1016/0016-7037(96)00209-8.

Xu, L., Lehmann, B., Mao, J., Qu, W., Du, A., 2011. Re-Os age of polymetallic Ni-Mo-PGE-Au mineralization in Early Cambrian black shales of South China—a reassessment. Econ. Geol. 106, 511–522. https://doi.org/10.2113/econgeo.106.3.511.

Yang, C., Zhu, M., Condon, D.J., Li, X., 2017. Geochronological constraints on stratigraphic correlation and oceanic oxygenation in Ediacaran-Cambrian transition in South China. J. Asian Earth Sci. 140, 75–81. https://doi.org/10.1016/j.jseaes.2017.03.017.

Zhang, Y., Zhang, Q., Cai, Y., Wang, D., Li, K., 2015. The occurrence state of vanadium in the black shale-hosted vanadium deposits in Shangling of Guangxi province, China. Chin. J. Geochem. 34, 484–497. https://doi.org/10.1007/s11631-015-0060-8.

Zhu, H., Ju, Y., Huang, C., Chen, F., Chen, B., Yu, K., 2020. Microcosmic gas adsorption mechanism on clay-organic nanocomposites in a marine shale. Energy 197, 1–16. https://doi.org/10.1016/j.energy.2020.117256.

Zimmerman, A.R., Chorover, J., Goyne, K., Brantley, S.L., 2004. Protection of mesopore-adsorbed organic matter from enzymatic degradation. Environ. Sci. Technol. 38, 4542–4548. https://doi.org/10.1021/es035340+.